

Series studies of the spin- $\frac{1}{2}$ Heisenberg antiferromagnet at $T=0$: Magnon dispersion and structure factors

Weihong Zheng,* J. Oitmaa,† and C. J. Hamer‡

School of Physics, The University of New South Wales, Sydney, NSW 2052, Australia.

(Received 7 December 2004; revised manuscript received 18 February 2005; published 31 May 2005)

We have extended our previous series studies of quantum antiferromagnets at zero temperature by computing the one-magnon dispersion curves and various structure factors for the linear chain, square, and simple cubic lattices. Many of these results are a substantial extension of previous work. These results are directly comparable to neutron-scattering experiments, and we make such comparisons where possible.

DOI: 10.1103/PhysRevB.71.184440

PACS number(s): 75.10.Jm, 75.50.Ee, 75.40.Gb

I. INTRODUCTION

The spin- $\frac{1}{2}$ Heisenberg antiferromagnet, which we take in the exchange anisotropic form

$$H = J \sum_{\langle ij \rangle} [S_i^z S_j^z + \lambda (S_i^x S_j^x + S_i^y S_j^y)], \quad |\lambda| \leq 1 \quad (1)$$

is the archetypal model for describing long-range antiferromagnetic order in solids. Although there are no exact solutions in greater than one spatial dimension, a great deal is known about the model from various systematic approaches: exact diagonalizations, quantum Monte Carlo methods, and series expansions. Good overviews of the subject, with a particular focus on the square lattice and the relation to the high T_c cuprate superconductors, have been given by Barnes¹ and Manousakis.² An area of particular current interest is the relation of models, such as (1), to real materials. Quantities that can be most readily compared are the dispersion relations of low-energy quasiparticle excitations and dynamical or integrated structure factors. The calculation of these is the main thrust of the current paper. At the same time the building of more powerful neutron-scattering facilities is providing more precise data and allowing more detailed comparisons between experiment and theory.³⁻⁵

Our approach is through high-order “linked-cluster” series expansions,⁶ where the quantities of interest are expanded perturbatively in powers of λ (the so-called Ising expansion) and numerically evaluated at $\lambda=1$. This approach has been used with considerable success in computing ground-state properties of quantum antiferromagnets⁷⁻⁹ and in computing the magnon excitation spectrum and spectral weight for the square lattice.¹⁰ In our calculations we set $J=1$ to determine the energy scale, except in comparisons with experiment. In Sec. II we will define the various quantities of interest and give a brief overview of the methodology. Section III gives results for the structure factors for the linear chain. Section IV extends previous work for the square lattice^{8,10} and gives results for the longitudinal and total structure factors. Section V gives results for the simple cubic lattice. Ground-state series are extended by two terms, and series results for the magnon energies and all structure factors are given. Finally, in Sec. VI we summarize and attempt to relate our work to experiment.

II. METHODOLOGY AND DEFINITIONS

The essence of the linked-cluster method⁶ is the realization that many properties of a lattice model, in the thermodynamic limit $N \rightarrow \infty$, can be expressed as a sum of contributions from all possible connected or linked clusters of sites that can be embedded in the particular lattice of interest. This is most obvious in the case of extensive bulk properties, such as the ground-state energy, magnetization, susceptibility, etc., where we have

$$F_N(x) = \sum_{\{g\}} C(g/\mathcal{L}) f_g(x), \quad (2)$$

where $F_N(x)$ is the quantity of interest, with x representing the set of parameters in the Hamiltonian. The sum is over all clusters $\{g\}$, with $C(g/\mathcal{L})$ being the embedding constant of cluster g in the lattice \mathcal{L} of N sites (proportional to N) and $f_g(x)$ a *reduced* quantity for cluster g . These latter quantities, which are independent of the lattice, are computed recursively.⁶ It is easy to show that $f_g(x)$ is zero for any disconnected cluster, provided F is an extensive quantity. Linked-cluster series expansions are then obtained by writing the Hamiltonian in the usual form for perturbation theory, $H=H_0+\lambda V$, and calculating the cluster contributions perturbatively, as series in λ , up to some maximum achievable order (typically 10–20). The bulk series for $F_N(\lambda)$ is then evaluated at fixed λ , or extrapolated to $\lambda=1$, via standard numerical methods, such as Padé approximants or integrated differential approximants.¹¹ In practice, all of this is done by computer and it is feasible to deal with of order 10^6 distinct clusters.

A stringent comparison between real materials and theoretical models is often provided by the spectrum of low-energy excitations. These excitation energies can be measured in scattering experiments and are characteristic of the quantum dynamics of the system. Gelfand¹² showed how to compute excitation energies perturbatively, within a linked-cluster approach, and this is now a standard technique.⁶ The basic idea is to (i) compute an *effective Hamiltonian* matrix, which operates in the subspace of one-particle excitations of a cluster, (ii) use this to obtain a set of *transition amplitudes* $t(\mathbf{r})$ that describe propagation of the excitation through a distance \mathbf{r} , (iii) obtain transition amplitudes for the bulk lattice by summing over clusters, and (iv) take the Fourier

transform, giving the excitation energy in \mathbf{k} space

$$\epsilon(\mathbf{k}) = \sum_{\mathbf{r}} t(\mathbf{r}) e^{i\mathbf{k}\cdot\mathbf{r}}. \quad (3)$$

Although the dispersion relation (3) is an important probe of the quantum dynamics, an even more comprehensive probe is the dynamical structure factor

$$S_{\alpha}(\mathbf{k}, \omega) = \frac{1}{2\pi} \int_{-\infty}^{\infty} dt e^{i\omega t} \sum_{\mathbf{r}} e^{i\mathbf{k}\cdot\mathbf{r}} \langle S_0^{\alpha}(0) S_{\mathbf{r}}^{\alpha}(t) \rangle_0, \quad (4)$$

i.e., the spatial and temporal Fourier transform of the dynamical spin-spin correlation function. The angular brackets denote an average (here a ground-state expectation value), and $\alpha=x, y, z$. This quantity is directly related to the cross section for inelastic neutron scattering (see, e.g., Ref. 13). The integrated or static structure factor

$$S_{\alpha}(\mathbf{k}) = \int_{-\infty}^{\infty} d\omega S_{\alpha}(\mathbf{k}, \omega) = \sum_{\mathbf{r}} e^{i\mathbf{k}\cdot\mathbf{r}} \langle S_0^{\alpha} S_{\mathbf{r}}^{\alpha} \rangle \quad (5)$$

is measured in an experiment where all neutron energies are included.

For an isotropic system, in the absence of long-range magnetic order or other spontaneously broken symmetry, the components $\alpha=x, y, z$ of $S_{\alpha}(\mathbf{k}, \omega)$ or $S_{\alpha}(\mathbf{k})$ will be equal. This will no longer be the case if magnetic order is present. For a collinear-ordered state, in the z direction, we need to distinguish between a *longitudinal* structure factor

$$S_l(\mathbf{k}) = \sum_{\mathbf{r}} e^{i\mathbf{k}\cdot\mathbf{r}} [\langle S_0^z S_{\mathbf{r}}^z \rangle - \langle S_0^z \rangle \langle S_{\mathbf{r}}^z \rangle] \quad (6)$$

and a *transverse* structure factor

$$S_t(\mathbf{k}) = \sum_{\mathbf{r}} e^{i\mathbf{k}\cdot\mathbf{r}} \langle S_0^x S_{\mathbf{r}}^x + S_0^y S_{\mathbf{r}}^y \rangle. \quad (7)$$

If unpolarized neutrons are used, the cross section will measure the total structure factor

$$S_{\text{tot}}(\mathbf{k}) = S_l(\mathbf{k}) + S_t(\mathbf{k}). \quad (8)$$

The dominant contribution to the transverse dynamical structure factor will come from one-magnon excitations, and $S_t(\mathbf{k}, \omega)$ will have the form

$$S_t(\mathbf{k}, \omega) = A_1(\mathbf{k}) \delta[\omega - \epsilon(\mathbf{k})] + S_{\text{inc}}(\mathbf{k}, \omega), \quad (9)$$

where $A_1(\mathbf{k})$ is called the one-magnon spectral weight (or the exclusive structure factor) and $S_{\text{inc}}(\mathbf{k}, \omega)$ is a smooth incoherent background term, arising from multimagnon processes. It is easy to show that

$$A_1(\mathbf{k}) = \frac{1}{2} \sum_{\mathbf{r}} e^{i\mathbf{k}\cdot\mathbf{r}} \langle \Psi_0 | (S_0^+ + S_0^-) | \Psi_{\mathbf{k}} \rangle \langle \Psi_{\mathbf{k}} | (S_{\mathbf{r}}^+ + S_{\mathbf{r}}^-) | \Psi_0 \rangle, \quad (10)$$

where $|\Psi_0\rangle, |\Psi_{\mathbf{k}}\rangle$ are, respectively, the ground state and one-magnon state and S_r^+, S_r^- are spin-raising and -lowering operators. It is also useful to define a relative multimagnon spectral weight by

$$W_l(\mathbf{k}) = 1 - A_1(\mathbf{k})/S_l(\mathbf{k}) \quad (11)$$

and a similar quantity for unpolarized neutron scattering

$$W_{\text{tot}}(\mathbf{k}) = 1 - A_1(\mathbf{k})/S_{\text{tot}}(\mathbf{k}). \quad (12)$$

The linked-cluster formalism to compute the structure factor is relatively straightforward and has been discussed in Refs. 14 and 10. The correlator sums

$$Z_{\alpha}(\mathbf{r}) \equiv \sum_i \langle S_i^{\alpha} S_{i+\mathbf{r}}^{\alpha} \rangle \quad (13)$$

are extensive quantities and, thus, have a linked-cluster expansion. There is, however, one interesting and important point regarding the longitudinal correlators and the structure factor. Linked-cluster series for the correlators $\langle S_0^z S_{\mathbf{r}}^z \rangle$, computed from a set of clusters up to some fixed maximum size, will have a maximum order in λ , which decreases with increasing \mathbf{r} . On the other hand, the series for the *compensated* correlator $\langle S_0^z S_{\mathbf{r}}^z \rangle - \langle S_0^z \rangle \langle S_{\mathbf{r}}^z \rangle$ has a maximum order independent of \mathbf{r} . This can be understood as follows. For any cluster the longitudinal correlator series all start with a constant (λ^0) term. Subtraction of subgraph contributions will cause cancellation of leading terms, leaving a series starting with some minimum power $\lambda^{p_{\text{min}}}$. However p_{min} decreases with increasing r and is zero for $r=r_{\text{max}}$, the largest correlator which fits into the cluster, since, in this case, there are no subgraph subtractions. Thus, in the absence of the compensating term (14), much larger clusters would be required to give the large- r correlator series to the same order. Inclusion of the compensating term avoids this problem since the leading terms in the bare correlator cancel and p_{min} (defined above), after subgraph subtraction, is independent of r . This allows longer series to be derived for the structure factor as defined in (6). The additional term

$$\sum_{\mathbf{r}} e^{i\mathbf{k}\cdot\mathbf{r}} \langle S_0^z \rangle \langle S_{\mathbf{r}}^z \rangle \quad (14)$$

will give a δ -function peak at the antiferromagnetic wave vector \mathbf{k}_{AF} , but will not change the longitudinal structure factor for $\mathbf{k} \neq \mathbf{k}_{\text{AF}}$. The inclusion of this term reduces the total longitudinal structure factor, summed over momentum \mathbf{k} , from S^2 to $S^2 - M^2$, where S and M are the spin and staggered magnetization, respectively. For the transverse structure factor this total sum is just S .

There are two methods for computing series for the one-magnon spectral weight $A_1(\mathbf{k})$. The first is to proceed directly from Eq. (10), as in Ref. 10. An alternate method¹⁴ is from the linked-cluster series for another quantity, the so-called exclusive matrix element,

$$\Omega(\boldsymbol{\delta}) = \langle \Psi_0 | (S_i^+ + S_j^-) | \Psi_m \rangle; \quad \boldsymbol{\delta} = \mathbf{r}_i - \mathbf{r}_m, \quad (15)$$

where $|\Psi_m\rangle$ is the one-magnon wave function with initial unperturbed excitation at site m . Then

$$A_1(\mathbf{k}) = \left| \sum_{\boldsymbol{\delta}} \Omega(\boldsymbol{\delta}) e^{i\mathbf{k}\cdot\boldsymbol{\delta}} \right|^2. \quad (16)$$

The advantage of this second method is that it can be easily extended to the two-particle case, although we do not pursue this here. The two methods should, of course, result in the

same final series. This provides a useful check on the correctness of the input cluster data, more stringent than the calculation of ground-state bulk properties or excitation spectra.

We compare our series results to the prediction from spin-wave calculations. For the anisotropic Hamiltonian (1), the spin-wave theory has been computed to fourth order for the ground-state energy and third order for most other properties.¹⁵ The second-order spin-wave theory predicts the spin-wave excitation spectrum

$$\epsilon_{\mathbf{k}} = zS q_{\mathbf{k}} - \frac{z}{2} [C_{-1} q_{\mathbf{k}} + (\lambda^{-2} - 1)(C_{-1} - C_1)(q_{\mathbf{k}}^{-1} - q_{\mathbf{k}})], \quad (17)$$

where z is the lattice coordination number, $q_{\mathbf{k}} = (1 - \lambda^2 \gamma_{\mathbf{k}}^2)^{1/2}$, C_n is defined as

$$C_n = \frac{2}{N} \sum_{\mathbf{k}} [(1 - \lambda^2 \gamma_{\mathbf{k}}^2)^{n/2} - 1], \quad (18)$$

and

$$\gamma_{\mathbf{k}} = \frac{1}{z} \sum_{\rho} e^{i\mathbf{k} \cdot \rho}. \quad (19)$$

At $\lambda=1$, we can get a simple expression for the excitation spectrum

$$\epsilon_{\mathbf{k}} = zS(1 - \gamma_{\mathbf{k}}^2)^{1/2} [1 - C_{-1}/(2S)]. \quad (20)$$

That is, the second-order spin-wave theory only gives an overall renormalization, with renormalization factor $Z_c = 1 - C_{-1}/(2S)$, to the dispersion given by linear spin-wave theory.

Linear spin-wave theory gives the transverse structure factor as

$$S_t(\mathbf{k}) = S \sqrt{\frac{1 - \lambda \gamma_{\mathbf{k}}}{1 + \lambda \gamma_{\mathbf{k}}}}. \quad (21)$$

In the limit $k = |\mathbf{k}| \rightarrow 0$, $\gamma_{\mathbf{k}} \rightarrow 1 - k^2/z$,

$$S_t(\mathbf{k}) = S \left(\frac{1 - \lambda}{1 + \lambda} + k^2 \frac{2\lambda}{(1 + \lambda)^2 z} \right)^{1/2} \quad (22)$$

so $S_t(\mathbf{k})$ vanishes as $S k / \sqrt{2z}$ at $\lambda=1$, while at $\mathbf{k}=0$, S_t vanishes as $S(1 - \lambda)^{1/2} / \sqrt{2}$ as $\lambda \rightarrow 1$.

In the limit $q \equiv |\mathbf{q}| = |\mathbf{k}_{\text{AF}} - \mathbf{k}| \rightarrow 0$, $\gamma_{\mathbf{k}} \rightarrow -1 + q^2/z$, and

$$1/S_t(\mathbf{k}) = S^{-1} \left(\frac{1 - \lambda}{1 + \lambda} + q^2 \frac{2\lambda}{(1 + \lambda)^2 z} \right)^{1/2} \quad (23)$$

so $S_t(\mathbf{k})$ diverges as $S \sqrt{2z}/q$ at $\lambda=1$, while at $\mathbf{k} = \mathbf{k}_{\text{AF}}$, S_t diverges as $S \sqrt{2}(1 - \lambda)^{-1/2}$ as $\lambda \rightarrow 1$.

We now turn to the series results.

III. THE LINEAR CHAIN

The anisotropic spin- $\frac{1}{2}$ Heisenberg antiferromagnet in one dimension (the XXZ chain) has been the subject of much study. Many materials, which are well represented by this

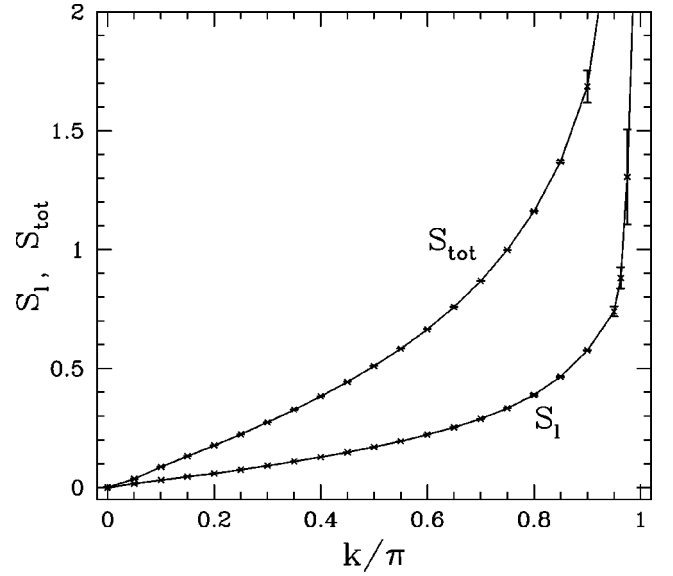


FIG. 1. The total and longitudinal structure factor for the linear chain.

model, have been identified (see Table 1 in Ref. 16). The possibility of exact results via Bethe ansatz methods has led to a good overall theoretical understanding of the model. In particular, it is known that the elementary excitations are $S = \frac{1}{2}$ spinons, or domain walls, with a dispersion relation¹⁸

$$\epsilon_{\text{spinon}}(k) = I [\cos^2(k) + g^2 \sin^2(k)]^{1/2}, \quad (24)$$

where

$$I = (1 - \lambda^2)^{1/2} K(g'^2) / \pi, \quad g'^2 = 1 = g^2 \quad (25)$$

and g is the solution of

$$\pi K(g^2) / K(g'^2) = \text{sech}^{-1}(\lambda) \quad (26)$$

and K denotes the complete elliptic integral,

$$K(x) = \int_0^{\pi/2} [1 - x \sin^2(\theta)]^{-1/2} d\theta. \quad (27)$$

A series expansion for the spinon energy has already been derived by Singh¹⁷ and shown to agree precisely with the expansion of the exact result (24) in powers of λ . The structure factors are not known exactly for the XXZ chain, and here series expansions have a role to play. Singh *et al.*¹⁹ obtained long series for the longitudinal and transverse structure factors (6) and (7) at the antiferromagnetic wave vector $k = \pi$, to 22 and 12 terms, respectively, in λ (only even terms occur in the longitudinal case) and studied the divergence of both quantities as $\lambda \rightarrow 1^-$. They found different exponents ($\sim 1.0, 0.75$) for the two power laws and explained this apparently surprising result via a renormalization-group argument.

We have computed series for all of the structure factors, for general wave vector k , to order λ^{28} . This represents 16 additional terms for the transverse (and hence the total) structure factor. Our results for the isotropic case ($\lambda=1$) are shown in Fig. 1. The structure factors diverge at $k = \pi$, as

expected. For $k \neq \pi$, we find, to numerical accuracy, that $S_{\text{tot}}=3S_1$, as expected, since the system has no long-range order. For $k=\pi$, our longer series also show that longitudinal and transverse structure factors diverge with two different exponents, as found by Singh *et al.*¹⁹

IV. THE SQUARE LATTICE

The square lattice $S=\frac{1}{2}$ antiferromagnet has been much studied in recent years, largely because of its relevance to the high T_c cuprate superconductors. There is convincing, though not yet rigorous, evidence that the ground state has long-range Néel order, reduced by quantum fluctuations.

Some years ago we derived⁸ perturbation series for the ground-state energy, sublattice magnetization, and parallel susceptibility to 14th order in the exchange anisotropic parameter λ , and for the transverse (perpendicular) susceptibility to order 13. These series provided very precise estimates of ground-state properties for the entire range $0 < \lambda \leq 1$, including the isotropic point $\lambda=1$. We also showed that higher-order spin-wave theory¹⁵ was in excellent agreement with the series results. We have recently extended these series by two terms, to order λ^{16} , the calculation involving a list of 185 690 clusters, up to 16 sites. We are happy to provide the coefficients on request, but do not present any analysis of ground-state properties here.

We have also extended an earlier calculation¹⁰ of the magnon excitation spectrum and spectral weight series by four terms, to order λ^{14} . This calculation involves a large list of 4 654 284 clusters, up to 15 sites. The series coefficients are quite extensive and are not presented here, but we will provide them on request. We give in Table I the series at $\mathbf{k}=(\pi, \pi)$, $(\pi, 0)$, and $(\pi/2, \pi/2)$. The resulting magnon dispersion curve is shown in Fig. 2. It was obtained by extrapolating the series to $\lambda=1$, using integrated differential approximants. The first-, second-, and third-order spin-wave results^{8,15} are included for comparison. We confirm the overall shape of the dispersion curve obtained previously¹⁰ but provide greater precision from the longer series. It is evident from the figure that the dispersion curve along the edge of the magnetic Brillouin zone $(\pi, 0) \rightarrow (\pi/2, \pi/2)$ is not flat, as predicted by the first- and second-order spin-wave theory. We find, numerically,

$$\epsilon(\pi, 0) = 2.18(1), \quad \epsilon(\pi/2, \pi/2) = 2.385(1), \quad (28)$$

and so there is a 9.4% increase from $(\pi, 0)$ to $(\pi/2, \pi/2)$. This agrees very well with a recent quantum Monte Carlo calculation²⁰ $\epsilon(\pi, 0)=2.16$, $\epsilon(\pi/2, \pi/2)=2.39$. Spin-wave theory, however, is unable to reproduce this variation even at third order,¹⁵ which gives $\epsilon(\pi, 0)=2.35858$, $\epsilon(\pi/2, \pi/2)=2.39199$. Our series results are also in qualitative agreement with experimental data for $\text{Cu}(\text{DCOO})_2 \cdot 4\text{D}_2\text{O}(\text{CFTD})^3$ and $\text{Sr}_2\text{Cu}_3\text{O}_4\text{Cl}_2^4$. However in La_2CuO_4 the observed magnon energy at $(\pi, 0)$ is higher than at $(\pi/2, \pi/2)$,⁵ opposite to the model result. It has been suggested⁵ that this is because of the presence of a significant ring exchange term in this material, but other explanations are possible.²¹

From our series for the magnon energies we can obtain a rather precise estimate of the spin-wave velocity v . Follow-

ing Singh and Gelfand¹⁰ we write the magnon energy at long wavelength in the form

$$\epsilon(\mathbf{k}) = C(\lambda) + D(\lambda)k^2 + O(k^3), \quad k = |\mathbf{k}| \rightarrow 0. \quad (29)$$

The spin-wave velocity v^2 can be obtained from the series for $2C(\lambda)D(\lambda)$, evaluated at $\lambda=1$. Using integrated differential approximants,¹¹ we estimate $2CD=2.774(6)$ at $\lambda=1$ and conclude that $v/Ja=1.666(2)$. For $\mathbf{k}=0$, we expect the spin-wave energy to vanish as

$$\epsilon(\mathbf{k}=0) = c(1 - \lambda^2)^{1/2}, \quad \lambda \rightarrow 1 - , \quad (30)$$

where the coefficient c can be estimated from our series: the result is $c=1.256(2)$. Third-order spin-wave theory¹⁵ gives $v/Ja=1.66802$ and $c=1.23531$, agreeing with the series estimates within 2%.

In Fig. 3 we show results for the various integrated structure factors along high symmetry lines in the Brillouin zone. The transverse structure factor was computed previously¹⁰ to order λ^{10} - we have extended this series by four terms, to order λ^{14} . Calculation of the longitudinal structure factor, and hence the total structure factor, by series methods is given here. The series at $\mathbf{k}=(\pi, \pi)$, $(\pi, 0)$, and $(\pi/2, \pi/2)$ are listed in Table I. Various features deserve comment. Both longitudinal and transverse structure factors vanish at $\mathbf{k}=(0, 0)$. It is known, on general grounds, that the k dependence at this point is k^2, k , respectively. Hence the longitudinal structure factor vanishes more rapidly. We estimate, from our series,

$$S_l(\mathbf{k}) = 0.042(4)k^2 \quad \text{as } k = |\mathbf{k}| \rightarrow 0 \quad (31)$$

$$S_t(\mathbf{k}) = 0.108(4)k \quad \text{as } k = |\mathbf{k}| \rightarrow 0, \quad (32)$$

where the coefficient for $S_l(\mathbf{k})$ is estimated using the same method as used for the spin-wave velocity v . A second-order spin-wave calculation²² gives $S_l(\mathbf{k})=0.10133k$.

Both structure factors diverge at the antiferromagnetic wave vector $\mathbf{k}=(\pi, \pi)$. If the Néel state were an exact eigenstate the static longitudinal structure factor would be zero, except for a δ -function peak at (π, π) . The actual shape reflects the additional contribution from quantum fluctuations. We first consider the asymptotic behavior of longitudinal and transverse static structure factors at $\mathbf{k}=(\pi, \pi)$, as $\lambda \rightarrow 1$. Assuming

$$S_l(\lambda) \sim (1 - \lambda)^{-\sigma_l}, \quad S_t(\lambda) \sim (1 - \lambda)^{-\sigma_t}, \quad (33)$$

we estimate, from biased Dlog Padé approximants, that $\sigma_l=0.50(2)$, while $\sigma_t=0.3(1)$. The exponents again differ, as in the one-dimensional (1D) case, but here it is σ_l that is apparently smaller (this could be related to the fact that $\langle S^z \rangle \neq 0$ on the square lattice). Linear spin-wave theory gives $\sigma_l=1/2$ [see Eq. (23)], but one would need a higher-order calculation to give σ_l . Next we consider the way in which the transverse and total structure factors at $\lambda=1$ diverge as $\mathbf{k} \rightarrow (\pi, -\pi)$. Defining $q=(\pi, \pi)-\mathbf{k}$, we write

$$S_t(\mathbf{q}) = C(\lambda) + D(\lambda)q^2 + O(q^3), \quad q = |\mathbf{q}| \rightarrow 0. \quad (34)$$

Both $C(\lambda)$ and $D(\lambda)$ diverge at $\lambda=1$. However if we compute the inverse

TABLE I. Series for the square lattice one-magnon dispersion $\epsilon(\mathbf{k})$, longitudinal structure factor $S_l(\mathbf{k})$, transverse structure factor $S_t(\mathbf{k})$, and one-magnon exclusive structure factor $A_1(\mathbf{k})$ at $\mathbf{k}=(\pi, \pi), (\pi, 0), (\pi/2, \pi/2)$, and series D for coefficient of k^2 (for ϵ and S_l) or q^2 (for S_t and A_1). Nonzero coefficients λ^n up to order $n=14$ are listed.

n	$\mathbf{k}=(\pi, \pi)$	$\mathbf{k}=(\pi, 0)$	$\mathbf{k}=(\pi/2, \pi/2)$	D
Dispersion $\epsilon(\mathbf{k})$				
0	2.000000000	2.000000000	2.000000000	0.000000000
2	-1.666666667	$3.333333333 \times 10^{-1}$	$3.333333333 \times 10^{-1}$	1.000000000
4	$3.171296296 \times 10^{-1}$	$-9.953703704 \times 10^{-2}$	$5.324074074 \times 10^{-2}$	$2.569444444 \times 10^{-1}$
6	$-4.192337641 \times 10^{-1}$	$-1.693897891 \times 10^{-3}$	$-9.073302469 \times 10^{-3}$	$6.581836259 \times 10^{-1}$
8	$2.709969904 \times 10^{-1}$	$-2.806720342 \times 10^{-2}$	$5.105325304 \times 10^{-3}$	$-4.886280904 \times 10^{-2}$
10	$-3.894335149 \times 10^{-1}$	$-1.062177000 \times 10^{-2}$	$2.076320167 \times 10^{-3}$	$7.984148319 \times 10^{-1}$
12	$4.289652578 \times 10^{-1}$	$-9.046042545 \times 10^{-3}$	$4.068538933 \times 10^{-4}$	$-5.057247719 \times 10^{-1}$
14	$-6.558882026 \times 10^{-1}$	$-8.872458632 \times 10^{-3}$	$1.304340621 \times 10^{-3}$	1.460095528
Longitudinal structure factor $S_l(\mathbf{k})$				
2	$2.222222222 \times 10^{-1}$	$1.111111111 \times 10^{-1}$	$1.111111111 \times 10^{-1}$	$2.777777778 \times 10^{-2}$
4	$7.358024691 \times 10^{-2}$	$-1.580246914 \times 10^{-2}$	$3.703703704 \times 10^{-4}$	$1.851851852 \times 10^{-3}$
6	$4.055166849 \times 10^{-2}$	$1.167542552 \times 10^{-2}$	$-1.111176199 \times 10^{-3}$	$3.826627719 \times 10^{-3}$
8	$3.646524757 \times 10^{-2}$	$1.065352379 \times 10^{-3}$	$4.750603835 \times 10^{-3}$	$2.311003576 \times 10^{-3}$
10	$2.483688972 \times 10^{-2}$	$2.298840789 \times 10^{-3}$	$1.379013443 \times 10^{-3}$	$1.874238376 \times 10^{-3}$
12	$2.211921434 \times 10^{-2}$	$1.532346963 \times 10^{-3}$	$1.422483566 \times 10^{-3}$	$1.550055137 \times 10^{-3}$
14	$1.886279612 \times 10^{-2}$	$1.141259073 \times 10^{-3}$	$1.002657611 \times 10^{-3}$	$1.314140042 \times 10^{-3}$
Transverse structure factor $S_t(\mathbf{k})$				
0	$5.000000000 \times 10^{-1}$	$5.000000000 \times 10^{-1}$	$5.000000000 \times 10^{-1}$	0.000000000
1	$6.666666667 \times 10^{-1}$	0.000000000	0.000000000	$-1.666666667 \times 10^{-1}$
2	$3.333333333 \times 10^{-1}$	$-1.111111111 \times 10^{-1}$	$-1.111111111 \times 10^{-1}$	$-2.222222222 \times 10^{-1}$
3	$2.648148148 \times 10^{-1}$	0.000000000	0.000000000	$-3.773148148 \times 10^{-1}$
4	$2.390123457 \times 10^{-1}$	$1.925925926 \times 10^{-2}$	$1.086419753 \times 10^{-2}$	$-4.340740741 \times 10^{-1}$
5	$2.157488242 \times 10^{-1}$	0.000000000	0.000000000	$-5.523841490 \times 10^{-1}$
6	$1.922286407 \times 10^{-1}$	$-1.297374724 \times 10^{-2}$	$-6.735355253 \times 10^{-3}$	$-6.036591991 \times 10^{-1}$
7	$1.825523316 \times 10^{-1}$	0.000000000	0.000000000	$-7.022537598 \times 10^{-1}$
8	$1.672647956 \times 10^{-1}$	$-2.593884626 \times 10^{-4}$	$-2.653241665 \times 10^{-3}$	$-7.488016779 \times 10^{-1}$
9	$1.584816304 \times 10^{-1}$	0.000000000	0.000000000	$-8.361027757 \times 10^{-1}$
10	$1.488115597 \times 10^{-1}$	$-2.819695062 \times 10^{-3}$	$-1.579465770 \times 10^{-3}$	$-8.786542283 \times 10^{-1}$
11	$1.436901069 \times 10^{-1}$	0.000000000	0.000000000	$-9.576556162 \times 10^{-1}$
12	$1.358134394 \times 10^{-1}$	$-1.233261351 \times 10^{-3}$	$-1.422867383 \times 10^{-3}$	$-9.970882006 \times 10^{-1}$
13	$1.316662910 \times 10^{-1}$	0.000000000	0.000000000	-1.069785636
14	$1.256571308 \times 10^{-1}$	$-1.266236691 \times 10^{-3}$	$-1.061011294 \times 10^{-3}$	-1.106759542
One-magnon spectral weight $A_1(\mathbf{k})$				
0	$5.000000000 \times 10^{-1}$	$5.000000000 \times 10^{-1}$	$5.000000000 \times 10^{-1}$	0.000000000
1	$6.666666667 \times 10^{-1}$	0.000000000	0.000000000	$-1.666666667 \times 10^{-1}$
2	$2.500000000 \times 10^{-1}$	$-1.388888889 \times 10^{-1}$	$-1.388888889 \times 10^{-1}$	$-1.944444444 \times 10^{-1}$
3	$1.425925926 \times 10^{-1}$	0.000000000	0.000000000	$-3.245370370 \times 10^{-1}$
4	$3.326195988 \times 10^{-1}$	$-1.143904321 \times 10^{-2}$	$1.529706790 \times 10^{-2}$	$-5.072723765 \times 10^{-1}$
5	$3.917638154 \times 10^{-1}$	0.000000000	0.000000000	$-6.858476264 \times 10^{-1}$
6	$3.936459588 \times 10^{-2}$	$-1.917201533 \times 10^{-2}$	$-1.696167024 \times 10^{-2}$	$-4.528242195 \times 10^{-1}$
7	$-8.018312217 \times 10^{-2}$	0.000000000	0.000000000	$-4.216442748 \times 10^{-1}$
8	$3.778813233 \times 10^{-1}$	$-1.855816875 \times 10^{-2}$	$-4.208337928 \times 10^{-3}$	-1.027026315
9	$5.220328525 \times 10^{-1}$	0.000000000	0.000000000	-1.343102568
10	$-1.799044627 \times 10^{-1}$	$-1.153727416 \times 10^{-2}$	$-3.162792993 \times 10^{-3}$	$-3.701268973 \times 10^{-1}$
11	$-4.037813448 \times 10^{-1}$	0.000000000	0.000000000	$-4.716188047 \times 10^{-2}$
12	$6.539878806 \times 10^{-1}$	$-9.013887872 \times 10^{-3}$	$-3.821489172 \times 10^{-3}$	-1.930735417
13	$9.853540532 \times 10^{-1}$	0.000000000	0.000000000	-2.711397791
14	$-7.366801888 \times 10^{-1}$	$-9.184484559 \times 10^{-3}$	$-1.633241155 \times 10^{-3}$	$6.457723508 \times 10^{-1}$

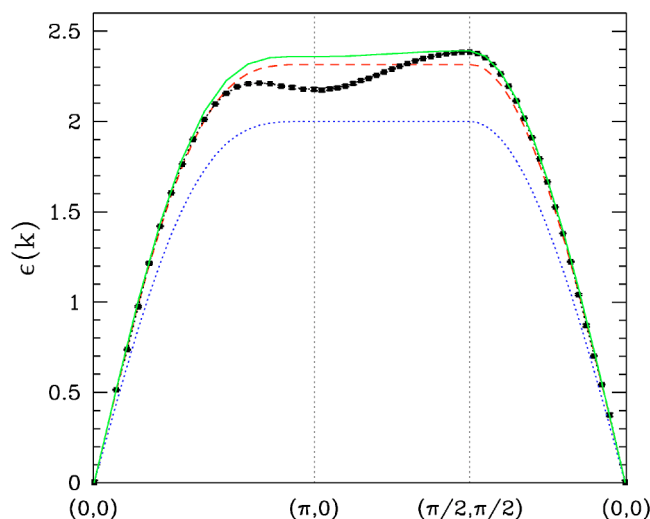


FIG. 2. (Color online) The one-magnon excitation spectrum $\epsilon(\mathbf{k})$ along high-symmetry cuts through the Brillouin zone for the Heisenberg antiferromagnet on a square lattice. Also shown are the results of first-order (blue dotted line), second-order (red dashed line), and third-order (green solid line) spin-wave theory.

$$1/S_t(\mathbf{q}) = 1/C(\lambda) - D(\lambda)q^2/C^2(\lambda) + O(q^3) \quad (35)$$

and compare to the asymptotic form (see Eq. (23))

$$1/S_t(\mathbf{q}) = [A(\lambda) + B(\lambda)q^2]^{1/2}, \quad (36)$$

we find that S_t diverges as $(B^{1/2}q)^{-1}$ with $B = -2D/C^3$. The series for D for S_t is given in Table I. Our series, when analyzed in this way, gives

$$S_t(q) = 0.93(7)/q, \quad q \rightarrow 0. \quad (37)$$

The total structure factor series gives an estimate of 0.95(5), consistent with the same result. Spin-wave theory²² gives 0.9288/ q .

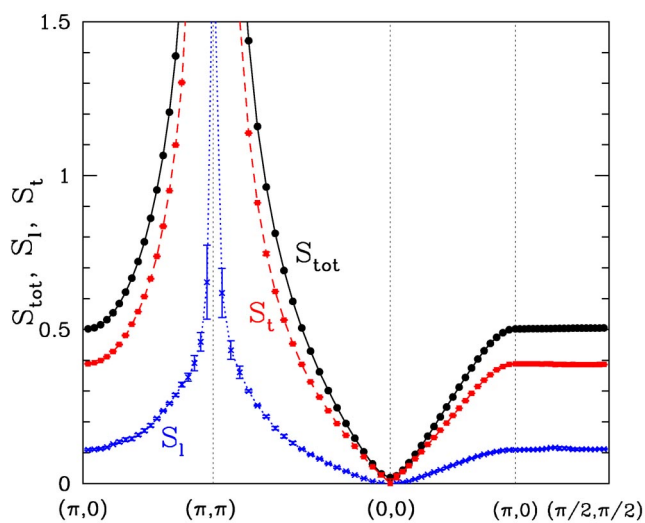


FIG. 3. (Color online) The various integrated structure factors S_{tot} (unpolarized), S_t (transverse), and S_l (longitudinal) along high-symmetry cuts through the Brillouin zone for the Heisenberg antiferromagnet on a square lattice.

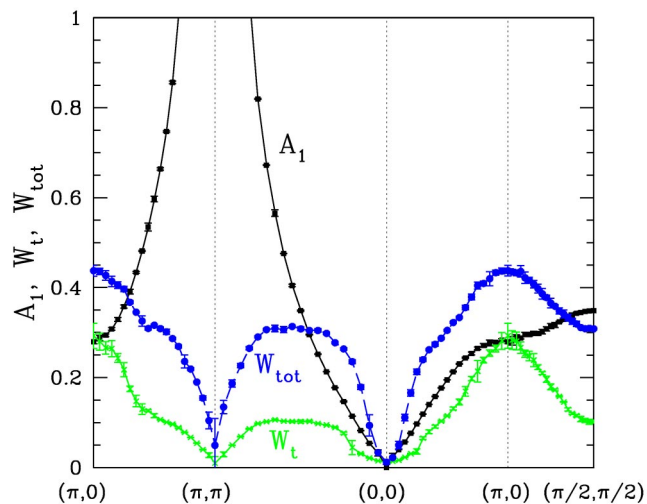


FIG. 4. (Color online) The one-magnon spectral weight A_1 , and multimagnon spectral weights W_t and W_{tot} for the Heisenberg antiferromagnet on a square lattice.

Finally we note that the transverse structure factor exceeds the longitudinal one throughout the zone. The dominant one-magnon states only contribute to the transverse structure factor. The data can be analyzed to extract the one-magnon spectral weight $A_1(\mathbf{k})$ and the relative multimagnon spectral weights [Eqs. (11) and (12)]. These are shown in Fig. 4, for the conventional lines in the Brillouin zone. The total one-magnon spectral weight, summed over \mathbf{k} , has the value 0.419(2), i.e., the one-magnon excitations contribute 0.419/0.5 \approx 84% of the total transverse weight. We note that the maximum multimagnon contribution to the structure factors, and, hence, to the integrated neutron-scattering intensity, occurs at the $(\pi, 0)$ point and is approximately 44% (29%) for unpolarized (polarized) neutrons. For $\mathbf{k} = (\pi/2, \pi/2)$, the multimagnon contribution is 31% (10%) for unpolarized (polarized) neutrons. Quantum Monte Carlo

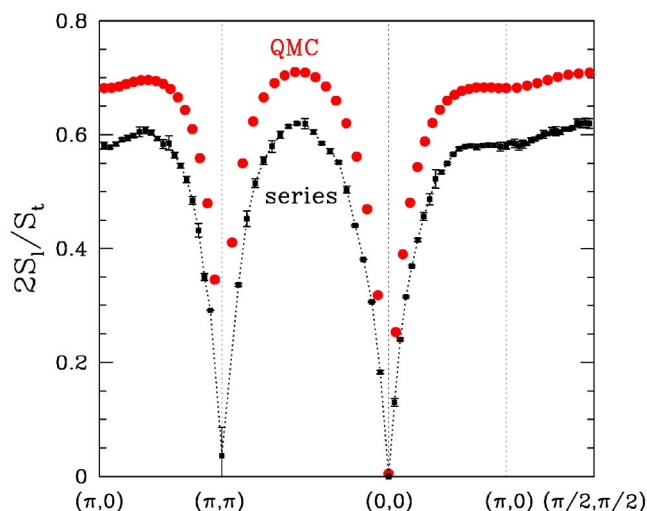


FIG. 5. (Color online) Ratio of longitudinal and transverse structure factors $2S_l/S_t$ for the Heisenberg antiferromagnet on a square lattice. Also shown, for comparison, are the QMC results (Ref. 20).

TABLE II. Series of simple cubic lattice one-magnon dispersion $\epsilon(\mathbf{k})$, longitudinal structure factor $S_l(\mathbf{k})$, transverse structure factor $S_t(\mathbf{k})$, and one-magnon exclusive structure factor $A_1(\mathbf{k})$ at $\mathbf{k}=(\pi, \pi, \pi), (\pi, 0, 0), (\pi/2, \pi/2, \pi/2)$, and series D for coefficient of k^2 (for ϵ and S_l) or q^2 (for S_t and A_1). Nonzero coefficients λ^n up to order $n=10$ are listed.

n	$\mathbf{k}=(\pi, \pi, \pi)$	$\mathbf{k}=(\pi, 0, 0)$	$\mathbf{k}=(\pi/2, \pi/2, \pi/2)$	D
Dispersion $\epsilon(\mathbf{k})$				
0	3.000000000	3.000000000	3.000000000	0.000000000
2	-1.950000000	$5.000000000 \times 10^{-2}$	$3.000000000 \times 10^{-1}$	$7.500000000 \times 10^{-1}$
4	$-7.480952381 \times 10^{-2}$	$5.483333333 \times 10^{-2}$	$-1.550595238 \times 10^{-3}$	$2.859821429 \times 10^{-1}$
6	$-2.386949857 \times 10^{-1}$	$-1.194666672 \times 10^{-2}$	$3.986473230 \times 10^{-3}$	$3.080615484 \times 10^{-1}$
8	$-3.884790029 \times 10^{-2}$	$2.654093113 \times 10^{-3}$	$6.579308964 \times 10^{-4}$	$1.842288801 \times 10^{-1}$
10	$-1.028725933 \times 10^{-1}$	$-5.327445001 \times 10^{-4}$	$5.131262221 \times 10^{-4}$	$2.278014891 \times 10^{-1}$
Longitudinal structure factor $S_l(\mathbf{k})$				
2	$1.200000000 \times 10^{-1}$	$4.000000000 \times 10^{-2}$	$6.000000000 \times 10^{-2}$	$1.000000000 \times 10^{-2}$
4	$1.684444444 \times 10^{-2}$	$-2.488888889 \times 10^{-3}$	$-3.962962963 \times 10^{-4}$	$1.530864198 \times 10^{-4}$
6	$1.301036907 \times 10^{-2}$	$2.757538780 \times 10^{-3}$	$2.815062245 \times 10^{-3}$	$8.063018305 \times 10^{-4}$
8	$8.184237447 \times 10^{-3}$	$7.116986056 \times 10^{-4}$	$1.126836657 \times 10^{-3}$	$3.866267816 \times 10^{-4}$
10	$6.005783346 \times 10^{-3}$	$6.521285585 \times 10^{-4}$	$8.514828105 \times 10^{-4}$	$3.009882557 \times 10^{-4}$
Transverse structure factor $S_t(\mathbf{k})$				
0	$5.000000000 \times 10^{-1}$	$5.000000000 \times 10^{-1}$	$5.000000000 \times 10^{-1}$	0.000000000
1	$6.000000000 \times 10^{-1}$	$-2.000000000 \times 10^{-1}$	0.000000000	$-1.000000000 \times 10^{-1}$
2	$3.000000000 \times 10^{-1}$	$-2.000000000 \times 10^{-2}$	$-6.000000000 \times 10^{-2}$	$-1.200000000 \times 10^{-1}$
3	$2.526666667 \times 10^{-1}$	$4.614814815 \times 10^{-2}$	0.000000000	$-1.887777778 \times 10^{-1}$
4	$2.137481481 \times 10^{-1}$	$-1.191111111 \times 10^{-2}$	$3.644444444 \times 10^{-3}$	$-2.033679012 \times 10^{-1}$
5	$2.025150853 \times 10^{-1}$	$-2.558718236 \times 10^{-3}$	0.000000000	$-2.520957812 \times 10^{-1}$
6	$1.752635491 \times 10^{-1}$	$-7.923299511 \times 10^{-4}$	$-3.718193643 \times 10^{-3}$	$-2.638276824 \times 10^{-1}$
7	$1.685481230 \times 10^{-1}$	$9.547987414 \times 10^{-4}$	0.000000000	$-3.039691386 \times 10^{-1}$
8	$1.523090399 \times 10^{-1}$	$-1.590182006 \times 10^{-3}$	$-9.298721272 \times 10^{-4}$	$-3.138723809 \times 10^{-1}$
9	$1.480721342 \times 10^{-1}$	$5.897338735 \times 10^{-4}$	0.000000000	$-3.487614896 \times 10^{-1}$
10	$1.365201003 \times 10^{-1}$	$-9.432640534 \times 10^{-4}$	$-8.927606509 \times 10^{-4}$	$-3.574938809 \times 10^{-1}$
One-magnon spectral weight $A_1(\mathbf{k})$				
0	$5.000000000 \times 10^{-1}$	$5.000000000 \times 10^{-1}$	$5.000000000 \times 10^{-1}$	0.000000000
1	$6.000000000 \times 10^{-1}$	$-2.000000000 \times 10^{-1}$	0.000000000	$-1.000000000 \times 10^{-1}$
2	$2.812500000 \times 10^{-1}$	$-2.875000000 \times 10^{-2}$	$-6.750000000 \times 10^{-2}$	$-1.162500000 \times 10^{-1}$
3	$2.251666667 \times 10^{-1}$	$5.309259259 \times 10^{-2}$	0.000000000	$-1.816944444 \times 10^{-1}$
4	$2.268800324 \times 10^{-1}$	$-1.446118552 \times 10^{-2}$	$1.009873984 \times 10^{-3}$	$-2.105439590 \times 10^{-1}$
5	$2.300857299 \times 10^{-1}$	$-5.633309085 \times 10^{-3}$	0.000000000	$-2.648295019 \times 10^{-1}$
6	$1.606446880 \times 10^{-1}$	$-2.164942522 \times 10^{-3}$	$-4.497506567 \times 10^{-3}$	$-2.550269987 \times 10^{-1}$
7	$1.424582061 \times 10^{-1}$	$2.355649892 \times 10^{-3}$	0.000000000	$-2.873096589 \times 10^{-1}$
8	$1.648269861 \times 10^{-1}$	$-2.195243132 \times 10^{-3}$	$-1.493247410 \times 10^{-3}$	$-3.243370831 \times 10^{-1}$
9	$1.707585298 \times 10^{-1}$	$2.315207796 \times 10^{-4}$	0.000000000	$-3.678986537 \times 10^{-1}$
10	$1.243609563 \times 10^{-1}$	$-1.435173150 \times 10^{-3}$	$-1.241136381 \times 10^{-3}$	$-3.458041669 \times 10^{-1}$

calculations²⁰ give 40% (15%) at $\mathbf{k}=(\pi, 0)$ [$\mathbf{k}=(\pi/2, \pi/2)$] for polarized neutrons. This is a significant contribution and needs to be allowed for in analysis of experimental data.

In Fig. 5 we plot the ratio $2S_l/S_t$ throughout the zone. The overall shape is in excellent agreement with recent Quantum Monte Carlo data,²⁰ but our maximum is about 0.62, considerably lower than the value 0.7 obtained by the Monte Carlo calculations.²⁰ Note that the quantum Monte

Carlo calculations have S_l/S_t diverging at $\mathbf{k}=(\pi, \pi)$, as they do not include the term (14) in their definition of the longitudinal structure factor. In principle, this term is a simple δ function at (π, π) and should not affect the measurement elsewhere for the bulk system. The omission of this term in the Monte Carlo calculations, however, can cause larger finite-size effects for finite systems, and this could be the cause of the discrepancy.

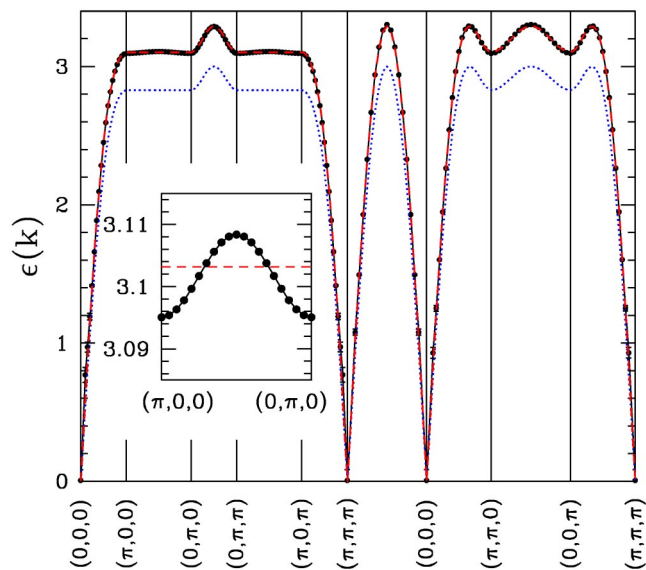


FIG. 6. (Color online) The one-magnon excitation spectrum $\epsilon(\mathbf{k})$ along high-symmetry cuts through the Brillouin zone for the Heisenberg antiferromagnet on the simple cubic lattice. Also shown are the results of first-order (blue dotted line) and second-order (red dashed line) spin-wave theory.

V. THE SIMPLE CUBIC LATTICE

We have carried out similar series calculations for the simple cubic lattice and report on these here. First, the previously calculated series for the ground-state properties⁹ have been extended by two terms, to order λ ,¹⁴ involving a list of 180 252 clusters, up to 14 sites. This does not significantly change the previous estimates of ground-state properties, and we do not present any further analysis. As usual, we

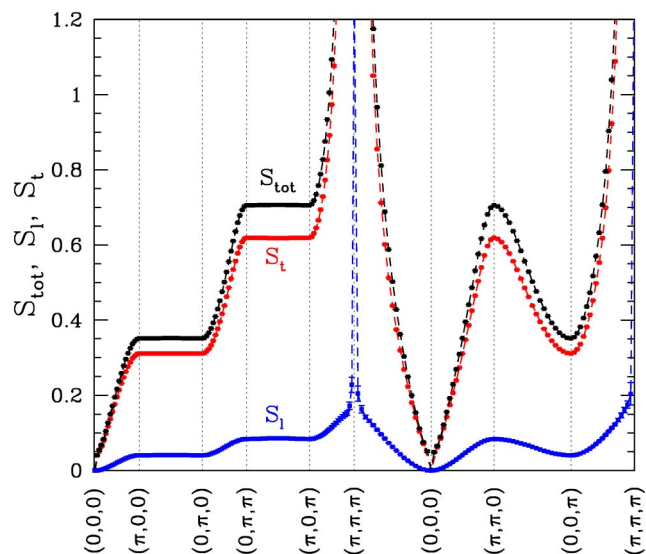


FIG. 7. (Color online) The various integrated structure factors S_{tot} (unpolarized), S_t (transverse), and S_l (longitudinal) along high-symmetry cuts through the Brillouin zone for the Heisenberg antiferromagnet on a simple cubic lattice.

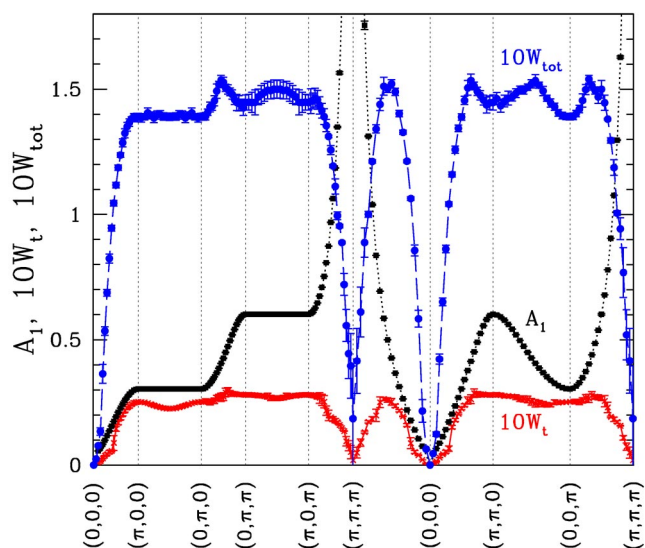


FIG. 8. (Color online) The one-magnon spectral weight A_1 , and multimagnon spectral weights W_t and W_{tot} for the Heisenberg antiferromagnet on the simple cubic lattice.

are happy to provide the coefficients to any interested reader.

Series for the magnon excitation spectrum have been derived to order λ^{10} . The calculations involve a list of 1 487 597 clusters, up to 11 sites. The series for $\mathbf{k} = (\pi, \pi, \pi), (\pi, 0, 0), (\pi/2, \pi/2, \pi/2)$ are given in Table II. Figure 6 shows the magnon excitation spectrum along high-symmetry lines through the Brillouin zone, obtained from the series expansion, and first- and second-order spin-wave theory. It is evident from the figure that first-order spin-wave theory gives the correct overall shape, but underestimates the magnitude by some 10%. The second-order spin-wave theory is virtually indistinguishable from the series data, except on an enlarged scale along some cuts (as shown in the inset). A calculation of the spin-wave velocity, along the same lines as

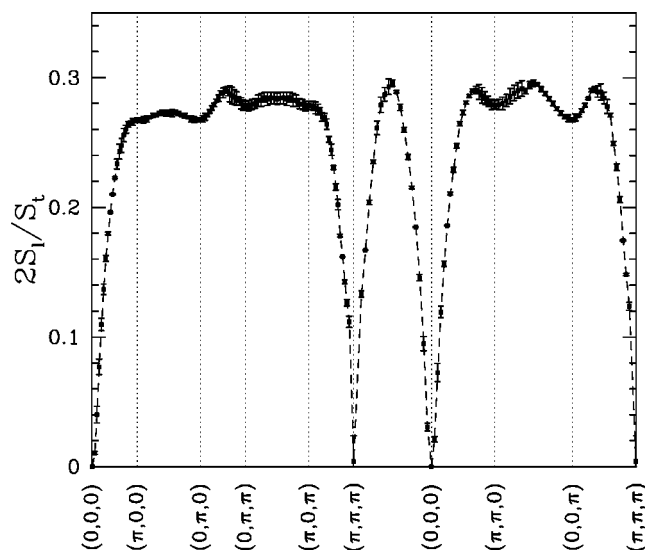


FIG. 9. Ratio of longitudinal and transverse structure factors $2S_l/S_t$ for the Heisenberg antiferromagnet on the simple cubic lattice.

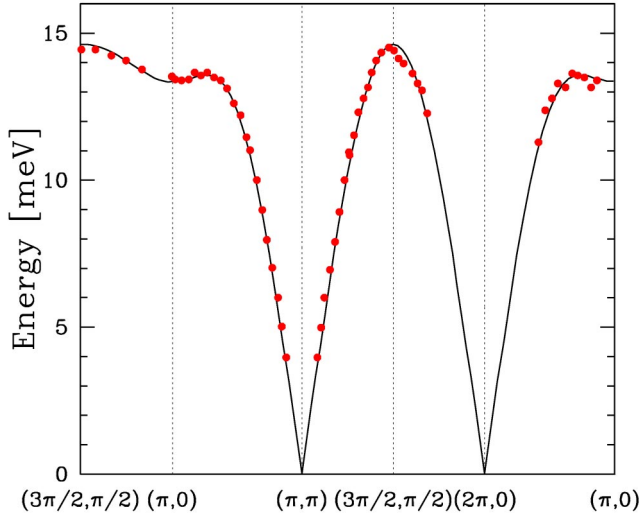


FIG. 10. (Color online) Comparison of the one-magnon dispersion for CFTD³ (red solid points) and our series results with $J = 6.13$ meV.

in Sec. IV, yields $v/Ja = 1.913(2)$. This compares to the first-(second-) order spin-wave value of $3^{1/2} = 1.732$ (1.9003) and yields a quantum renormalization factor of $Z = 1.104(1)$ [compared to the square lattice with $Z = 1.178(2)$]. This again is totally consistent with the lower relative effect of quantum fluctuations in higher dimensions.

Figure 7 gives our series estimates of the integrated structure factors along symmetry lines in the simple cubic Brillouin zone. These are obtained from series expansions to order λ .¹⁰ The same observations made for the square lattice can be made here. We note that the antiferromagnetic peak in S_l is noticeably sharper here than for the square lattice, again reflecting the reduced role of quantum fluctuations. Finally in Fig. 8 we show the one-magnon spectral weight and the relative multimagnon spectral weights. The latter are magnified by a factor of 10 for greater clarity. The multimagnon con-

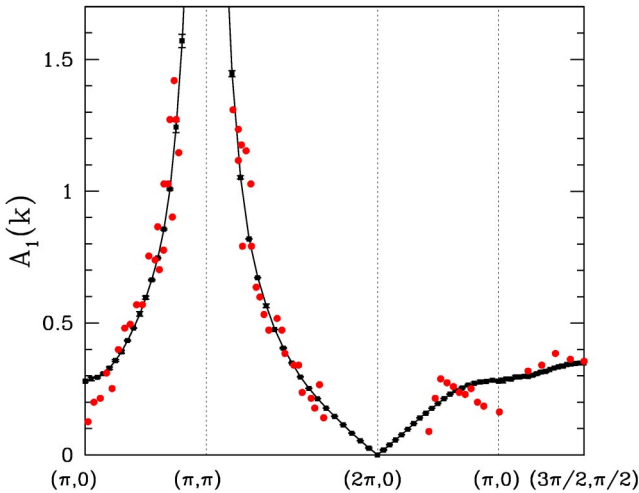


FIG. 11. (Color online) Comparison of the one-magnon transverse structure factor $A_1(\mathbf{k})$ for CFTD³ (red solid points) and our series results.

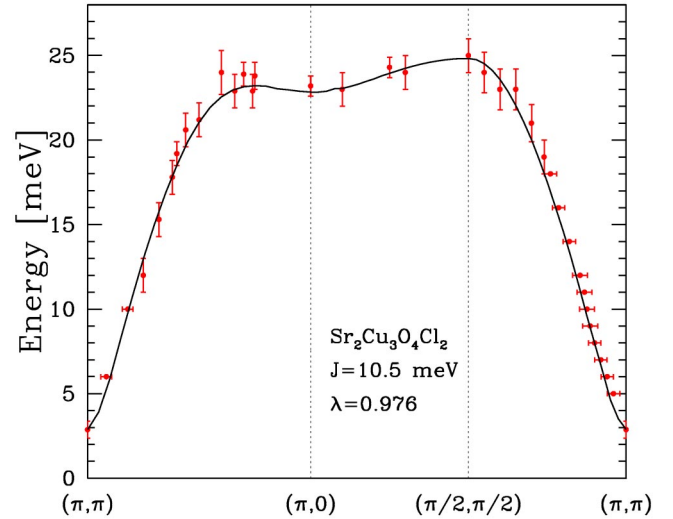


FIG. 12. Comparison of the one-magnon dispersion for $\text{Sr}_2\text{Cu}_3\text{O}_4\text{Cl}_2$ ⁴ and our series results with $J = 10.5$ meV, $\lambda = 0.976$.

tribution to the transverse structure factor is nowhere greater than 3%, indicating the dominance of one-magnon states, whereas the multimagnon contribution to the total structure factor, as would be measured by unpolarized neutrons, is as much as 15%. The total one-magnon spectral weight, summed over \mathbf{k} , has the value 0.482(1), i.e., the one-magnon excitations contribute 96.4% of the total transverse weight.

Similarly to the square lattice case, we obtain the following asymptotic results near $\mathbf{k} = 0$ and (π, π, π) :

$$S_l(\mathbf{k}) = 0.0114(2)k^2, \quad \mathbf{k} \rightarrow 0, \quad (38)$$

$$S_l(\mathbf{k}) = 0.1204(9)k, \quad \mathbf{k} \rightarrow 0, \quad (39)$$

$$S_t(\mathbf{q}) = 1.47(3)/q, \quad \mathbf{q} \rightarrow 0. \quad (40)$$

Estimates from the S_{tot} series are consistent with these.

In Fig. 9 we plot the ratio $2S_l/S_t$ throughout the zone. Here it has a maximum value about 0.3, substantially smaller than for the square lattice. We are unaware of any calculations of this ratio by other methods.

VI. SUMMARY AND DISCUSSIONS

The goal of this work has been to obtain numerically precise estimates of magnon energies and structure factors for the nearest-neighbor spin- $\frac{1}{2}$ Heisenberg antiferromagnet for the linear chain ($d=1$), square ($d=2$), and simple cubic ($d=3$) lattices. These quantities are directly comparable to experimental neutron-scattering results, and the resulting comparison can provide a stringent test of the applicability of the simple model, as well as yielding an estimate of the (usually unknown) parameter J .

We present such a comparison here for the quasi-two-dimensional materials deuterated copper formate tetrahydrate $(\text{CuDCOO})_2 \cdot 4\text{D}_2\text{O}$ (CFTD)³ and the so-called 2342 compound $\text{Sr}_2\text{Cu}_3\text{O}_4\text{Cl}_2$.⁴ CFTD is a well-characterized 2- d antiferromagnet.³ Figures 10 and 11 show a fit of our theo-

retical dispersion curve (Fig. 2) and one-magnon transverse structure factor $A_1(\mathbf{k})$ to the experimental data,³ with a parameter $J=6.13$ meV. The overall agreement is very good, except near $\mathbf{k}=(\pi,0)$, where the theoretical one-magnon transverse structure factor is higher than the experimental results. The fitting parameter J is in good agreement with an earlier fit³ to the previous series results.¹⁰ The strontium material is, *a priori*, more complex.⁴ It contains two types of Cu^{2+} ions, Cu_I and Cu_{II} , and the interaction between these is fully frustrated. To the extent that one can regard these subsystems as decoupled, the Cu_{II} subsystem can be treated as an effective spin- $\frac{1}{2}$ square lattice antiferromagnet with $J \sim 10$ meV. The measured dispersion curve shows a small spin gap, which can be modeled via a small magnetic anisotropy in the Hamiltonian. Figure 12 shows a comparison between the experimental data and our series results with $J = 10.5$ meV, $\lambda=0.976$, where λ is determined from the minimum gap using Eq. (30). As is evident the fit is excellent and again corroborates earlier results.⁴ One should be cautious, however, in claiming too much from this, and it would be highly desirable to have detailed structure factor data for further comparisons to be made.

We are unaware of any good examples of spin- $\frac{1}{2}$ antiferromagnetic materials with a simple cubic structure. Our results confirm, as expected, that the relative effect of quantum

fluctuations decreases with increasing spatial dimension. Nevertheless, the multimagnon contributions to integrated structure factors, and, hence, to neutron scattering intensities, can still be appreciable even in three dimensions.

For dimensions 2 and 3, the series expansion results are in very good agreement with spin-wave theory, as far as it has been calculated. We conclude that the spin-wave calculations should be extended to higher order, to further check the agreement in quantities, such as the longitudinal structure factor, which have been little studied as yet.

Note added. Recently, we became aware of the work by Igarashi and Nagao,²³ who have performed a second-order spin-wave calculation of the transverse structure factor for the square lattice.

ACKNOWLEDGMENTS

We are grateful to Professor Rajiv Singh, Professor T. Barnes, Professor R. Coldea, and Professor A. Sandvik for useful correspondences. This work forms part of a research project supported by a grant from the Australian Research Council. We are grateful for the computing resources provided by the Australian Partnership for Advanced Computing (APAC) National Facility and by the Australian Centre for Advanced Computing and Communications (AC3).

*Electronic address: w.zheng@unsw.edu.au

†Electronic address: j.oitmaa@unsw.edu.au

‡Electronic address: c.hamer@unsw.edu.au

¹T. Barnes, *Int. J. Mod. Phys. C* **2**, 659 (1991).

²E. Manousakis, *Rev. Mod. Phys.* **63**, 1 (1991).

³N. B. Christensen, D. F. McMorrow, H. M. Ronnow, A. Harrison, T. G. Perring, and R. Coldea, *J. Magn. Magn. Mater.* **272–276**, 896 (2004); H. M. Ronnow, D. F. McMorrow, R. Coldea, A. Harrison, I. D. Youngson, T. G. Perring, G. Aeppli, O. Syljuasen, K. Lefrann, and C. Rischel, *Phys. Rev. Lett.* **87**, 037202 (2001).

⁴Y. J. Kim, R. J. Birgeneau, F. C. Chou, M. Greven, M. A. Kastner, Y. S. Lee, B. O. Wells, A. Aharony, O. Entin-Wohlmann, I. Ya. Korenblit, A. B. Harris, R. W. Erwin, and G. Shirane, *Phys. Rev. B* **64**, 024435 (2001).

⁵R. Coldea, S. M. Hayden, G. Aeppli, T. G. Perring, C. D. Frost, T. E. Mason, S. W. Cheong, and Z. Fisk, *Phys. Rev. Lett.* **86**, 5377 (2001).

⁶M. P. Gelfand and R. R. P. Singh, *Adv. Phys.* **49**, 93 (2000).

⁷R. R. P. Singh, *Phys. Rev. B* **39**, R9760 (1989).

⁸W. Zheng, J. Oitmaa, and C. J. Hamer, *Phys. Rev. B* **43**, 8321 (1991).

⁹J. Oitmaa, C. J. Hamer and W. Zheng, *Phys. Rev. B* **50**, 3877 (1994).

¹⁰R. R. P. Singh, *Phys. Rev. B* **47**, 12 337 (1993); R. R. P. Singh and M. P. Gelfand, *ibid.* **52**, R15 695 (1995).

¹¹A. J. Guttman, in *Phase Transitions and Critical Phenomena*, edited by C. Domb and J. Lebowitz (Academic, New York, 1989), Vol. 13.

¹²M. P. Gelfand, *Solid State Commun.* **98**, 11 (1996).

¹³C. Broholm and G. Aeppli, in *Strong Interactions in Low Dimensions (Physics and Chemistry of Materials with Low Dimensional Structures)*, edited by D. Baeriswyl and L. Degiorgi (Kluwer, Dordrecht, 2004).

¹⁴W. Zheng, C. J. Hamer, and R. R. P. Singh, *Phys. Rev. Lett.* **91**, 037206 (2003); C. J. Hamer, W. Zheng, and R. R. P. Singh, *Phys. Rev. B* **68**, 214408 (2003).

¹⁵C. J. Hamer, W. Zheng, and P. Arndt, *Phys. Rev. B* **46**, 6276 (1992); W. Zheng and C. J. Hamer, *ibid.* **47**, 7961 (1993).

¹⁶C. Broholm, G. Aeppli, Y. Chen, D. C. Dender, M. Enderle, P. R. Hammar, Z. Honda, K. Katsumata, C. P. Landee, M. Oshikawa, L. P. Regnault, D. H. Reich, S. M. Shapiro, M. Sieling, M. B. Stone, M. M. Turnbull, I. Zaliznyak, and A. Zheludev, in *High Magnetic Fields - Applications in Condensed Matter Physics and Spectroscopy*, edited by C. Berthier, L. P. Lévy, and G. Martinez (Springer-Verlag, Berlin, 2002), pp. 211–234.

¹⁷R. R. P. Singh, *Phys. Rev. B* **53**, 11 582 (1996).

¹⁸J. D. Johnson, S. Krinsky and B. M. McCoy, *Phys. Rev. A* **8**, 2526 (1973); M. Mohan and G. Müller, *Phys. Rev. B* **27**, 1776 (1983).

¹⁹R. R. P. Singh, M. E. Fisher and R. Shankar, *Phys. Rev. B* **39**, 2562 (1989).

²⁰A. W. Sandvik and R. R. P. Singh, *Phys. Rev. Lett.* **86**, 528 (2001).

²¹N. M. R. Peres and M. A. N. Araújo, *Phys. Rev. B* **65**, 132404 (2002).

²²C. M. Canali and M. Wallin, *Phys. Rev. B* **48**, 3264 (1993).

²³J. Igarashi and T. Nagao, cond-mat/0502318 (unpublished).